

Low PAPR MIMO-OFDM Design Based on Convolutional Autoencoder

Yara Huleihel, and Haim H. Permuter, *Senior Member, IEEE*

Abstract

An enhanced framework for peak-to-average power ratio (PAPR) reduction and waveform design for Multiple-Input-Multiple-Output (MIMO) orthogonal frequency-division multiplexing (OFDM) systems, based on a convolutional-autoencoder (CAE) architecture, is presented. The end-to-end learning-based autoencoder (AE) for communication networks represents the network by an encoder and decoder, where in between, the learned latent representation goes through a physical communication channel. We introduce a joint learning scheme based on projected gradient descent iteration to optimize the spectral mask behavior and MIMO detection under the influence of a non-linear high power amplifier (HPA) and a multipath fading channel. The offered efficient implementation novel waveform design technique utilizes only a single PAPR reduction block for all antennas. It is throughput-lossless, as no side information is required at the decoder. Performance is analyzed by examining the bit error rate (BER), the PAPR, and the spectral response and compared with classical PAPR reduction MIMO detector methods on 5G simulated data. The suggested system exhibits competitive performance when considering all optimization criteria simultaneously. We apply gradual loss learning for multi-objective optimization and show empirically that a single trained model covers the tasks of PAPR reduction, spectrum design, and MIMO detection together over a wide range of SNR levels.

Index Terms

Deep learning, Autoencoder, Multiple-Input-Multiple-Output, Orthogonal frequency-division multiplexing, Peak-to-average power ratio, Wireless signal processing.

I. INTRODUCTION

The Multiple-input-multiple-output (MIMO) scheme is a widely used technique for enhancing channel capacity and transmission reliability, thanks to the diversity and multiplexing gains. Orthogonal frequency division multiplexing (OFDM) is a waveform design method known for providing high bandwidth efficiency, high throughput, simple equalization in wireless transmission, and efficient hardware implementation. For these reasons, it has been adopted as a standard technology in various wireless communication systems, such as WiFi, 4G, and 5G standards for wireless communications. Nonetheless, significant drawbacks of the OFDM multi-carrier system appear in the form of adjacent channel power ratio (ACPR) limitations and the tendency to produce signals with a high peak-to-average power ratio (PAPR) in the time-domain, since many subcarrier components are added via a fast Fourier transform (FFT) operation. The contribution of each subcarrier to the total power is dynamic, which makes the total power highly variable. In particular, the high PAPR in MIMO-OFDM systems is exacerbated as the number of antennas increases [1]. The demand for higher energy efficiency as well as reduced power consumption is expected to increase for future radio systems [2]. Moreover, future communication system design and equipment are expected to be more compatible with machine learning (ML) implementation requirements, for example, allowing learning in the field to make some design choices [2]. Accordingly, waveform designs using ML techniques are becoming significantly attractive.

A high power amplifier (HPA) is required to provide enough output power for reliable communication. In practical systems, the HPA is not linear and distorts the transmitted signal. As a result, severe non-linear signal distortions are found when these high PAPR signals pass through the non-linear HPA. The resulting signal exhibits spectral regrowth in the form of in-band signal distortions and out-of-band radiation [3], and the bit error rate (BER) increases. Hence, it is crucial to develop PAPR reduction techniques for MIMO-OFDM systems to increase their efficiency in handling large data streams and to reduce their error rates. Training and applying

the PAPR reduction block to each antenna individually exacerbates the complexity, cost, and redundancy in proportion to the number of transmit antennas in the system. Instead, in this work, a single PAPR reduction block jointly operates on all antenna OFDM sequences, and it is designed according to the maximum PAPR value of all antenna sequences.

A central difficulty of the multiple transmitter (TX) and receiver (RX) antenna structure is posed by the need for joint detection of the data symbols sent by each transmitter. Unfortunately, the optimal MIMO detection solution imposes an NP-hard problem on the receiver. Consequently, various sub-optimal yet feasible detection algorithms have been proposed. Other than classical model-driven solutions, an increasing effort has been dedicated to ML, and, specifically, deep learning (DL) based techniques to solve the MIMO detection problem, and more generally, various wireless communication tasks.

The design of OFDM waveform signals aims to simultaneously achieve a high data rate, high spectral efficiency (measured by the ACPR), and low computational complexity [4], [5]. This design is highly affected by the non-linear effects of the HPA. While keeping the PAPR level low is favorable, it is of particular importance to have acceptable signal spectral behavior and BER, which are often referred to as *waveform design*. In order to fulfill that, this work suggests an overall communication network multi-objective optimization, such that the transmitter, HPA, channel, and the receiver, are represented as a single optimization block. Instead of separately optimizing different components of the transmitter and the receiver, an end-to-end convolutional-autoencoder (CAE) learning model is proposed. This end-to-end optimization block is presented as a constrained optimization problem where the transmitted signal estimation is the objective, and the PAPR and ACPR requirements are the constraints. MIMO detection over multiple channel realizations is performed as a part of the end-to-end joint optimization model, utilizing an iterative approach based on convolutional layers, and a gradual loss learning approach. We evaluate the performance of our algorithms over both additive white Gaussian noise (AWGN) and 3rd Generation Partnership Project (3GPP) fading channels [6]. By analyzing the BER, PAPR, and

spectrum performance, we show that the proposed end-to-end learning approach can integrate different communication network blocks to balance those performance objectives successfully. We show that the suggested scheme is able to achieve better spectral performance for higher HPA efficiency operation. Various OFDM PAPR reduction techniques have been proposed in the literature, as well as for MIMO detection. Generally, these techniques can be categorized into *model-driven* and *data-driven* techniques. The first category refers to standard approaches in classical communications theory, while the second relies on recently developed approaches based on ML techniques. The following subsections review different earlier solutions for the above-mentioned problems.

A. Classical Approaches (Model Driven) for MIMO Detection

Many MIMO detection algorithms have been developed over the years. The maximum likelihood estimation (MLE) solution is optimal for the joint detection of transmitted symbols in a MIMO system. However, its exponential computational and time complexity (due to exhaustive searches over all possible transmitted signals) render it infeasible when the number of transmitters and the modulation order are high. An example of suboptimal high accuracy non-linear detection algorithms are those based on sphere decoding (SD) [7], but they become computationally expensive as the number of antennas grows. The general idea is based on a lattice search for a solution in an iterative manner, and the accuracy/complexity ratio strongly depends on the value chosen for the radius parameter. More advanced detectors include the successive interference cancellation (SIC) based detectors [8] and the semi-definite relaxation detectors [9].

B. Machine-Learning-Based Schemes (Data Driven) for MIMO Detection

The motivation for DL-based detectors is to enhance the performance of classical model-driven detection algorithms by learning, from the training data set, an optimized mapping of the received signals onto the transmitted symbols. In [10], [11], an iteration-based algorithm for implementing a receiver for MIMO detection was suggested. One of the highlights of the

presented model's framework is that it enables training through different random communication channel realizations. In [12], a model-based algorithm was suggested, where a classical SD algorithm was integrated with a neural network (NN) that was trained to optimize the selection of the initial radius. In [13], a neural detector-based transformer architecture implements a recurrent estimation scheme by learning an iterative decoding algorithm.

In [14]–[16] an AE was offered to design a physical layer in which DL-based CSI encoding was suggested for different scenarios to achieve lower BER together with better robustness to the wireless channel characteristics. Thorough surveys and analysis are presented in [17].

C. Classical Approaches (Model Driven) for PAPR Reduction

PAPR reduction schemes are roughly classified into three categories. The signal distortion category consists of techniques such as clipping and filtering (CF) [18], [19], which limit the peak envelope of the input signal in the time domain to a predetermined value. The multiple signaling probabilistic category includes methods such as selective mapping (SLM) [19], [20], partial transmit sequence (PTS) [20], ton reservation and ton injection [21], and constellation shaping [22]. The main principle of SLM is to generate different candidates for each OFDM block by multiplying the symbols vector with a set of different pseudo-random sequences and choosing the candidate with the lowest PAPR. The third category is the coding technique category [21], [23], attempting to reduce the occurrence probability of the same phase signals.

Earlier schemes were mainly developed for single-antenna systems. Extended works which applied the single-antenna PAPR reduction schemes on each antenna of the MIMO configuration separately are found in, e.g., [24], but those required considerable computations, cost, and complexity. Model-driven approaches to simultaneously reduce PAPR over all antennas were also proposed. In [25], instead of applying SLM to each antenna, the sequence with the highest PAPR over all transmit antennas was selected. Usually, SLM and PTS methods demand side information (SI) to be sent to the receiver along with each transmitted data block for retrieving the original data. The need for SI requires extra bandwidth overhead, and the incorrect detection

of the SI bits over the channel will lead to significant degradation in the BER performance of the receiver in the MIMO-OFDM system.

D. Deep-Learning-Based Schemes (Data Driven) for PAPR Reduction

In recent years much research has been dedicated to applying DL techniques in the design and optimization of wireless communication networks, e.g., [4], [11], [26]. Several papers have proposed DL methods to handle PAPR reduction. For example, the authors of [27], [28], added a NN to reduce the complexity of the active constellation scheme, followed by CF. In [29], [30] the authors present an AE solution for PAPR reduction, while minimizing the BER degradation. In [31] a CAE was suggested for the implementation of an end-to-end SISO – OFDM communication network that simultaneously reduces the PAPR and reconstructs the transmitted symbols, while keeping acceptable spectral requirements. Another learning-based approach, which considers the reduction of the PAPR and ACPR together with the maximization of the achievable information rate for a single-carrier waveform above multipath channels, was proposed in [32]. The authors in [33] proposed a deep NN combined with SLM to mitigate the high PAPR issue of OFDM signal types.

All of the above papers consider a SISO network. A PAPR reduction scheme assisted by DL for a MIMO-OFDM system was suggested in [34]. The authors apply selective tone reservation [35] on each antenna separately and then apply unused beam reservation [36] on all antennas together. An ML-based method for approximating the optimal tabular hyperparameters required for using selective tone reservation and unused beam reservation was suggested.

E. Main Contributions

Some of the aforementioned PAPR reduction approaches suffer from in-band interference, out-of-band distortions, and high computational complexity. Moreover, published ML-based solutions mostly handle single antenna scenarios. Those who deal with PAPR reduction for MIMO systems use ML only for the PAPR reduction block and not for the end-to-end network implementation. This paper aims to handle the PAPR problem in MIMO systems as an integral part of a waveform

design objective. In particular, we design a communication system that simultaneously achieves PAPR reduction, acceptable spectral behavior of the PA's output, and good BER performance. The suggested end-to-end network aims to resolve the MIMO detection problem as a part of the other mentioned objectives. To the best of our knowledge, this approach is new. Novelties we introduce include using a CAE combined with a gradual loss learning technique to handle the multi-objective optimization of the network, and adding the effect of the HPA on an integrated end-to-end MIMO communication system. We present an iterative MIMO detection algorithm integrated into transmitter-receiver end-to-end communication system joint optimization. We demonstrate our algorithm's results on 5G MIMO-OFDM Matlab toolbox simulated data, and we compare our method with classical methods for PAPR reduction and waveform design, and show competitive results for all the objectives mentioned above. The proposed algorithm offers performance improvement for future wireless communication systems. We show that our model provides competitive PAPR reduction, waveform design, and detection results.

The rest of this paper is structured as follows. In Section II, the problem is defined and formulated separately for MIMO detection, and for PAPR reduction as a part of the MIMO-OFDM system. We then present the proposed DL-based system architecture for the multi-objective optimization and explain the training procedure in Section III. Section IV provides detailed numerical simulation results and insights. Finally, Section V gives concluding remarks.

II. NOTATION AND PROBLEM DEFINITION

In this section, we introduce the notation and the problem definition.

A. Notation

Throughout this paper, we use the following notations. The set of real numbers is denoted by \mathbb{R} , while the set of complex numbers is denoted by \mathbb{C} . Random variables will be denoted by capital letters, and their realizations will be denoted by lower-case letters, e.g., X and x , respectively. Calligraphic letters denote sets, e.g., \mathcal{X} . We use the notation X^n to denote the random vector (X_1, X_2, \dots, X_n) and x^n to denote the realization of such a random vector.

The expectation operator is denoted by $\mathbb{E}[\cdot]$. $(\cdot)^*$, $(\cdot)^\dagger$ denote the conjugate, and pseudo-inverse operators, respectively.

B. Problem Definition

In this section, we describe mathematically each part of the integrated problem of MIMO detection together with PAPR reduction and spectrum constraints. First, we give a brief introduction to the end-to-end setup used in our system.

1) *MIMO detection model*: Let us assume a standard MIMO-OFDM system with N_t transmit antennas and N_r receive antennas. Transmission is considered over a memoryless complex-valued channel model, while assuming frequency flatness and slow fading. A MIMO system can be modeled by the following complex baseband model:

$$\mathbf{y} = \mathbf{H}\mathbf{x} + \mathbf{n}, \quad (1)$$

where $\mathbf{x} \in \mathbb{C}^{N_t}$ is the transmitted complex symbol vector drawn from a finite discrete constellation of size $|\mathcal{M}|$, $\mathbf{H} \in \mathbb{C}^{N_r \times N_t}$ is the complex baseband channel matrix that is related to a specific subcarrier, $\mathbf{n} \in \mathbb{C}^{N_r}$ is complex background AWGN seen at the receiver, and $\mathbf{y} \in \mathbb{C}^{N_r}$ is the received complex vector resulting from the propagation of the transmitted symbols through the channel contaminated by AWGN.

As the proposed implementation is based on a real-valued NN model determined by the DL Pytorch library, (1) is expressed with real values by splitting and concatenating each signal into its real and imaginary parts:

$$\mathbf{x} = \begin{bmatrix} \text{Re}\{\mathbf{x}\} \\ \text{Im}\{\mathbf{x}\} \end{bmatrix}, \quad \mathbf{y} = \begin{bmatrix} \text{Re}\{\mathbf{y}\} \\ \text{Im}\{\mathbf{y}\} \end{bmatrix}, \quad \mathbf{n} = \begin{bmatrix} \text{Re}\{\mathbf{n}\} \\ \text{Im}\{\mathbf{n}\} \end{bmatrix}, \quad \mathbf{H} = \begin{bmatrix} \text{Re}\{\mathbf{H}\} & -\text{Im}\{\mathbf{H}\} \\ \text{Im}\{\mathbf{H}\} & \text{Re}\{\mathbf{H}\} \end{bmatrix}. \quad (2)$$

In the MIMO detection problem, the objective is to detect the transmitted symbols, \mathbf{x} , given the received data \mathbf{y} . The optimal solution for the MIMO detection of the transmitted symbols problem defined above is given by the MLE algorithm, that is,

$$\hat{\mathbf{x}}_{mle} = \arg \min_{\mathbf{x} \in \mathcal{X}^{N_t}} \|\mathbf{y} - \mathbf{H}\mathbf{x}\|^2, \quad (3)$$

where \mathcal{X} denotes the set of possible transmitted symbols (i.e., signal constellation). The solution of (3) requires an exhaustive search over all $|\mathcal{M}|^{N_t}$ possible transmitted vectors. Therefore, it is infeasible for an actual implementation where large-scale MIMO setups and/or a large constellation are in use.

2) *PAPR problem in MIMO-OFDM*: In an OFDM system with N complex orthogonal sub-carriers, the discrete-time transmitted OFDM signal at the n_t antenna, is given by the inverse discrete Fourier transform (IDFT):

$$x_{n_t,n} = \frac{1}{\sqrt{N}} \sum_{k=0}^{N-1} X_{n_t,k} e^{j \frac{2\pi}{LN} kn}, \quad 0 \leq n \leq LN - 1, \quad 1 \leq n_t \leq N_t, \quad (4)$$

where $\{X_{n_t,k}\}_{k=0}^{N-1}$ are random input symbols per antenna, modulated by a finite constellation, and $L \geq 1$ is the over-sampling factor ($L = 1$ is the Nyquist sampling rate). As shown in [21], oversampling by a factor of four results in a good approximation of the continuous-time PAPR of complex OFDM signals. The discussed problem considers non-linear HPAs at each of the N_t TX branches. We assume that the HPAs in all branches have the same non-linear characteristic, which is a reasonable assumption, considering current wireless MIMO systems. Also, in a discrete implementation, the same HPAs are usually used.

The PAPR of the transmitted signal in (4) is defined as the ratio between the maximum peak power and the average power of the OFDM signal. Specifically, the PAPR at the n_t -th transmit antenna is defined by:

$$\text{PAPR}_{n_t} \triangleq \frac{\max_{0 \leq n \leq LN-1} |x_{n_t,n}|^2}{\mathbb{E}|x_{n_t,n}|^2}. \quad (5)$$

For the entire MIMO-OFDM system, the PAPR reduction method we use will consider the maximum PAPR among all N_t transmit antennas, as the same PA model is used in all branches:

$$\text{PAPR}_{\text{MIMO-OFDM}} = \max_{1 \leq n_t \leq N_t} \text{PAPR}_{n_t}. \quad (6)$$

As HPA non-linearity causes spectral regrowth, an important assessment for the spectral purity of the system is the ACPR criterion, which is the ratio between the power of the adjacent channel

and the power of the main channel. Following [6], we define it as

$$\text{ACPR} \triangleq \frac{\max \left(\int_{\text{BW}/2}^{3\text{BW}/2} P_{\text{ss}}(f) df, \int_{-3\text{BW}/2}^{-\text{BW}/2} P_{\text{ss}}(f) df \right)}{\int_{-\text{BW}/2}^{\text{BW}/2} P_{\text{ss}}(f) df}, \quad (7)$$

where $P_{\text{ss}}(\cdot)$ is the power spectral density (PSD) of the signal at the HPA's output, and BW is the primary channel bandwidth, which is assumed to be equal to the data signal bandwidth.

A block diagram of the communication system model is shown in Fig. 1.

Specifically, the encoder and filter blocks mitigate the PAPR effect and design the waveform to comply with predefined spectral mask requirements. For example, the encoder block can model a clipping

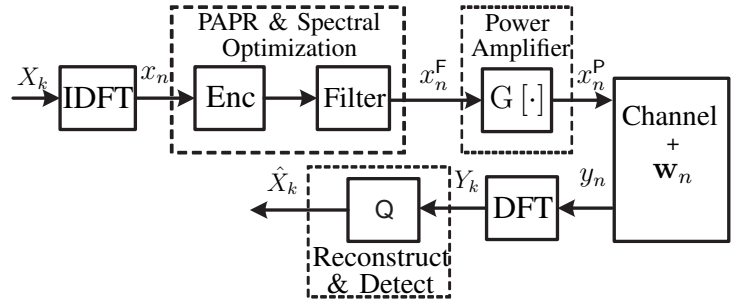


Fig. 1: General system model diagram.

operation, while the filter can be a standard band-pass filter (BPF). The filtered signal x_n^F is amplified by a non-linear HPA. The amplified signal, $x_n^P = G(x_n^F)$, is transmitted through a fading channel with AWGN. The channel decoder receives the noisy signal and attempts to reconstruct and detect the transmitted signal. For model-driven approaches, a classical detection algorithm, e.g., MLE, is applied for detecting the estimated symbol denoted by \hat{X}_k .

The role of the HPA is to convert the low-level transmission signal to a high power signal, capable of driving the antenna at the desired power level. The HPA has to operate close to its saturation region for maximal power efficiency. If the HPA exceeds the saturation point and enters the non-linear area of operation, the output signal becomes non-linear. Accordingly, to operate the amplifier only in the linear region, we need to make sure that the amplifier operates at a power level that is lower than the saturation point. This is achieved by down-scaling the input signal by an input back-off (IBO) factor. The drawback of adding the IBO attenuation is that the output power decreases, which makes the HPA power-inefficient.

There are several commonly used models for the non-linearity of an HPA. Here, we will focus on the RAPP behavioral amplifier model [37], which is very accurate for solid-state-power amplifiers. The model's AM/AM conversion is given by

$$G(A_{in}) = v \cdot A_{in} \cdot \left(1 + \left(\frac{v A_{in}}{A_0} \right)^{2p} \right)^{-\frac{1}{2p}}, \quad (8)$$

where A_{in} is the input amplitude, A_0 is the limiting output amplitude, v is the small signal gain, p is a smoothness parameter controlling the transition from the linear region to the saturation region, and $G(A)$ is the output amplitude. Figure 2 shows RAPP HPA outputs versus input for several smoothing factor values.

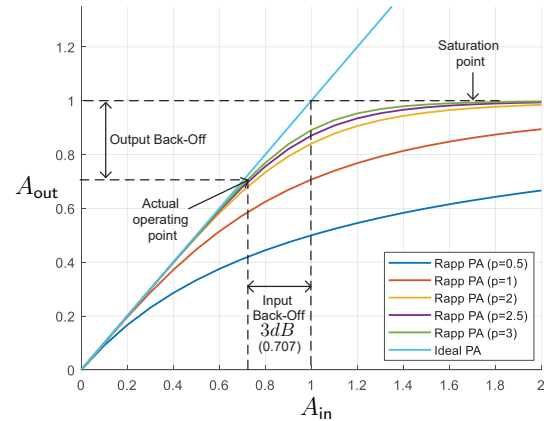
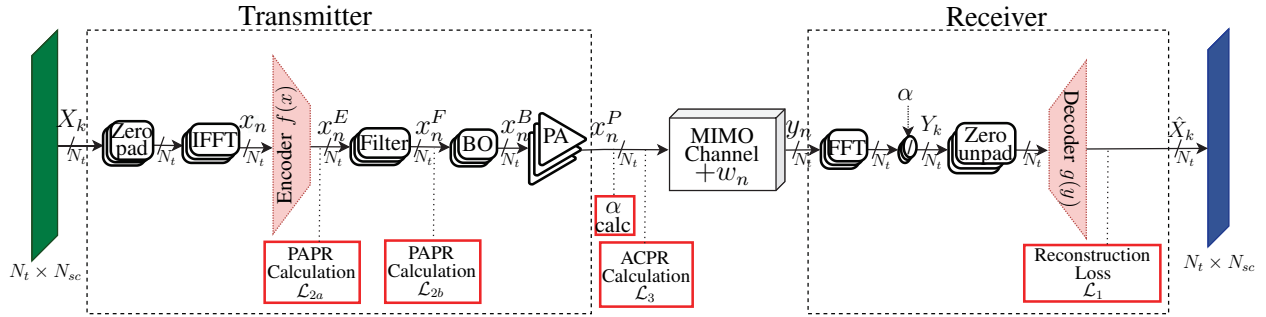


Fig. 2: RAPP HPA output versus input signal for different smoothness p values.

III. PROPOSED WAVEFORM DESIGN STRUCTURE

In this section, we describe our multi-objective optimization CAE model architecture. Motivated by research evidence of powerful learning ability, under the same conditions of the MIMO-OFDM examined structure, it is expected that the proposed CAE model will achieve good enough performance to be compared with classical PAPR reduction methods combined with the MLE detector. We first briefly discuss the general CAE concept. Then, we describe our algorithm building blocks, and the joint PAPR reduction, spectral design, and detection operation in detail. The motivation and structure of the iteration-based decoder with regard to handling the MIMO detection problem as a part of the CAE network will be explained. The proposed architecture in Fig. 3 is then elaborated, including the Bussgang's non-linearity compensation theorem, followed by a description of the gradual learning process. Last, the training procedure of the CAE multi-objective optimization network operation will be described.

Fig. 3a shows the overall end-to-end communication network structure implemented by a CAE model, where the encoder and the decoder are the trainable blocks. Each mentioned loss



(a) Conv-AE overall scheme.

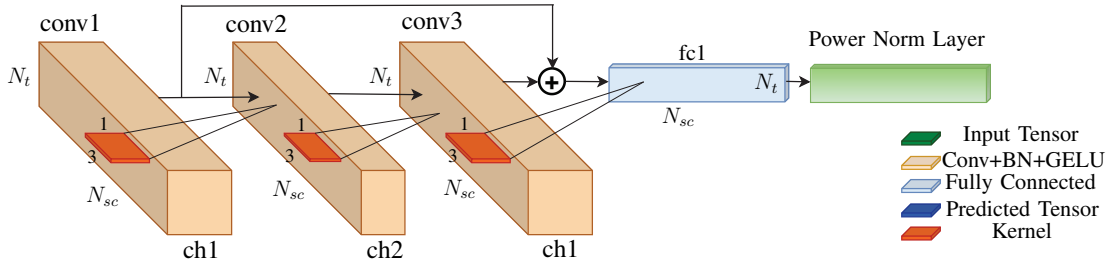
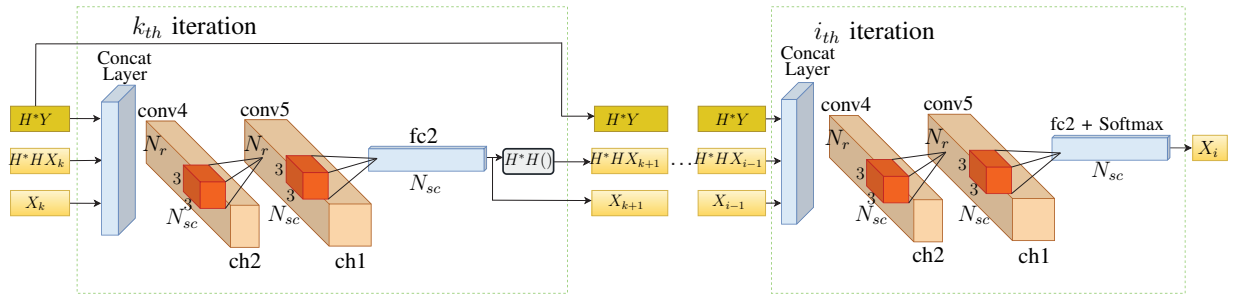
(b) PAPR reduction block - Encoder scheme $f(x)$.(c) Detection block - Decoder scheme $g(x)$.

Fig. 3: Structure of the proposed conv-AE.

component is calculated using the operations appearing in the red blocks in the figure. It can be noticed that there are two PAPR calculation-based loss components, as will be detailed later, that helped achieve improved spectral behavior and BER results. Fig. 3b describes the encoder structure. It is constructed of 2D convolutional layers to be compatible with the input example dimensions, a fully connected layer, and a power normalization layer at the output. We also added a skip connection to improve stability and performance. Fig. 3c shows the decoder structure. It is also implemented with 2D convolutional layers. To be able to optimize the network under

different communication channel realizations, we used an iterative-based solution to the MIMO detection problem. We emphasize that the presented CAE model, once trained on a single training set, presents competitive results for the discussed multi-objective optimization problem in the presence of a wide range of noise power levels, without any knowledge of the SNR level.

A. Convolutional Autoencoder (CAE)

The proposed implementation uses an AE learning system based on a convolutional neural network (CNN). The general structure of an AE consists of two main blocks: the encoder $f(\mathbf{x})$ and the decoder $g(\mathbf{x})$, where \mathbf{x} is the input data. The AE is trained to minimize a certain joint loss function, which we denote by $\mathcal{L}(\mathbf{x}, g(f(\mathbf{x})))$. An end-to-end communication system can be interpreted as an AE in which the encoder and the decoder are part of the transmitter and the receiver, respectively, and can jointly optimize them through an end-to-end learning procedure.

CNNs are widely used for feature extraction and pattern recognition in ML models. Compared with a fully connected (FC) network, a CNN has significantly fewer connections between adjacent layers, and thus fewer parameters and weights to train, resulting in lower complexity and much faster training.

B. Iteration-Based Model Motivation

An iterative approach based on convolutional layers, was adopted to implement the decoder. The MIMO detector was designed to solve the MLE optimization (3) using the projected gradient descent approach, where the input to the detector is a linear combination of features instead of the channel output directly. Utilizing such detectors significantly improved the detection results when various channel realizations were integrated. The detector input feature selection was based on the following projected gradient decent approach used to optimize (9):

$$\|\mathbf{y} - \mathbf{H}\mathbf{x}\|^2. \quad (9)$$

As shown in [10], [11], such iterations are updated by

$$\hat{\mathbf{x}}_{k+1} = P_c \left[\hat{\mathbf{x}}_k - \delta_k \frac{\partial \|\mathbf{y} - \mathbf{H}\mathbf{x}\|^2}{\partial \mathbf{x}} \Big|_{\mathbf{x}=\hat{\mathbf{x}}_k} \right] = P_c \left[\hat{\mathbf{x}}_k - \delta_k (\mathbf{H}^H \mathbf{y} - \mathbf{H}^H \mathbf{H} \hat{\mathbf{x}}_k) \right], \quad (10)$$

where $\hat{\mathbf{x}}_k$ is the objective estimation in the k 'th iteration, \mathbf{H}^H indicates the conjugate transpose operation over the channel matrix \mathbf{H} , δ_k is the step size, and P_c is the non-linear projection operator. The above can be adapted to a deep NN iterative solution by the following linear combination form:

$$\hat{\mathbf{x}}_{k+1} = P_c(\hat{\mathbf{x}}_k + \delta_{1k}\mathbf{H}^H\mathbf{y} + \delta_{2k}\mathbf{H}^H\mathbf{H}\hat{\mathbf{x}}_k), \quad (11)$$

where δ_{1k} and δ_{2k} are learned hyper-parameters to be optimized. One of the motivations for using the described iterative decoder approach was a former work published in [10], [11]. In our work, it is designed as part of the joint encoder-decoder multi-task optimization. Also, it was implemented with convolutional layers, that enabled better computational and performance capabilities for the joint optimization end-to-end system, and the per subcarrier/antenna alternating analysis. A softmax layer is added at the output of the CAE to generate probabilistic outputs. In the following section, we provide the complete detection procedure.

C. Proposed CAE Architecture

This section introduces the suggested CAE learning network implementation of the MIMO-OFDM system for the multi-objective optimization task. We consider a MIMO-OFDM scheme with N_t transmit antennas and N_r receive antennas, where the OFDM is of order K . The input is represented by a matrix in the frequency domain, i.e.

$$\underline{\mathbf{X}} = \begin{pmatrix} X^{(1)}(1) & X^{(1)}(2) & \dots & X^{(1)}(K) \\ X^{(2)}(1) & X^{(2)}(2) & \dots & X^{(2)}(K) \\ \vdots & \vdots & \ddots & \vdots \\ X^{(N_t)}(1) & X^{(N_t)}(2) & \dots & X^{(N_t)}(K) \end{pmatrix}, \quad (12)$$

where, for any $n_t \in [1, N_t]$ and $k \in [1, K]$, $X^{(n_t)}(k)$ is a M-QAM constellation complex-valued symbol.

In Fig. 3a, we illustrate the general structure of the end-to-end communication network implemented by the CAE configuration. Specifically, we consider a transmitter that takes the

two-dimensional matrix $\underline{\mathbf{X}}$ as an input. The transmitter's output goes through a MIMO channel, together with AWGN. Finally, the noisy channel outputs are fed into a receiver to estimate $\underline{\mathbf{X}}$. The operations within the transmitter and the receiver are described below.

- **Transmitter:** the input signal $\underline{\mathbf{X}}$ is zero-padded on the subcarriers' dimension and converted to the time domain via an IFFT applied on each of the transmitter branches, outputting $\{x_n\}_{n=0}^{LN-1}$. These symbols serve as the input to the encoder, which acts as a PAPR reduction block, followed by a BPF filter for optimizing the spectral behavior by reducing the out-of-band radiation. Its frequency response is a rectangular window with the same bandwidth as $X_k^{(n_t)}$. Then, a predefined IBO is applied just before the signal is amplified by the HPA.
- **Receiver:** the distorted OFDM symbols are divided by an α factor to compensate for the non-linear distortions, as will be detailed in the following. Finally, the proposed CAE decoder reconstructs and detects the estimated MIMO-OFDM transmitted signals.

The encoder comprises three convolutional layers, and the decoder is composed of iterative construction of convolutional layers. Each convolutional layer is followed by a non-linear activation function and batch normalization [38], and then a fully connected layer. In addition, a residual connection is added to the encoder block, which sums (element-wise) the input to the second convolutional layer and the output of the third convolutional layer. It turns out that this modification improves the overall performance of the suggested scheme significantly. The intuition is that adding another path for data to reach the latter parts of the NN makes it easier to optimize the mapping [39]. Furthermore, the encoder has a power normalization layer, which ensures that the transmitted signal meets the power constraints of unit average energy per OFDM symbol. This way, the intended SNR is maintained. We tested several activation functions, including sigmoid, rectified linear unit (RELU), Gaussian error linear unit (GELU), and scaled exponential linear unit (SELU) [40]. Empirically, it was found that SELU activation provides the best results for our CAE scheme.

As illustrated in Fig. 3a and Fig. 3b, since the encoder is responsible for the PAPR reduction,

which is calculated per OFDM symbol, we start with per antenna analysis, where each antenna is treated separately. A one-dimensional kernel per TX branch handles this. The encoder architecture can be described by the following:

$$f(\mathbf{x}) = \rho_{L_f} \left(\left| \mathbf{W}_{L_f}^f \left(\rho_{L_f-1} \left(\dots \left(\rho_1 \left(\left| \mathbf{W}_1^f \mathbf{x} + \mathbf{b}_1^f \right|_{bnorm} \right) \right) \dots \right) \right) \right|_{bnorm} + \left| \mathbf{W}_1^f \mathbf{x} + \mathbf{b}_1^f \right|_{bnorm} \right), \quad (13)$$

where L_f is the number of the encoder's convolutional layers, \mathbf{W}_i^f , and \mathbf{b}_i^f are the encoder's weight matrix and bias vector, respectively, for the i 'th layer, with size determined as a part of the network design. $\rho_i(\cdot)$ is the activation function of the i 'th layer, and $bnorm$ means the layer passes through a batch normalization.

The next part of this process applies the non-linear HPAs on each TX branch of the transmitter time domain signals, each composed of all subcarriers. The signal is then converted via FFT to the frequency domain, and the zero-unpadding block removes the out-of-band samples. Afterward, frequency domain analysis is performed on each subcarrier transmitted through all N_t antennas. Each subcarrier is transmitted through its related complex baseband channel described by a $(N_r \times N_t)$ matrix, and the AWGN is added as well.

To continue with the per subcarrier analysis on the receiver side, we need to overcome the non-linearity of the HPA. To that end, we compensate the receiver input signal by applying an attenuation factor represented by α . Bussgang's decomposition theorem [41] states that if a zero-mean Gaussian signal passes through a memoryless non-linear device, then the output-input cross-correlation function is proportional to the input autocovariance. Accordingly, the value of α is chosen to minimize the variance of the non-linear signal distortions, such that it is attempted that the transmitted signal in each transmitter branch is linearly separated, and thus represented as a sum of the signal and distortion. It can be shown that

$$\alpha = \frac{\mathbb{E}(x_n^F \bar{x}_n^F)}{\mathbb{E}(|x_n^F|^2)}, \quad (14)$$

where x_n^P is the complex output signal of the PA, and \bar{x}_n^P is its complex conjugate. By assuming that the PSD of the in-band distortion is approximately flat [42] in the frequency domain, the output signal of the HPA on the k -th subcarrier can then be expressed as

$$X^P(k) = \alpha(k)X^F(k) + D(k), \quad (15)$$

where $D(k)$ is the non-linear distortion on the k -th subcarrier. The same model is assumed for all PAs; therefore, it can be concluded that $\alpha_{n_t} = \alpha$.

At the MIMO decoder, Fig. 3c, the per subcarrier analysis is continued, meaning that different subcarriers of the same RX branch will not be mixed. To generalize our end-to-end structure, we modified the 1D kernel to a 2D kernel at the decoder part. It also helped better reconstruct the signal after the encoder layers. As explained in the previous sub-section, we use an iterative procedure to implement the decoder, which is designed for signal reconstruction and detection. A general mathematical description of one iteration, k , of the presented decoder is given by

$$\mathbf{d}_k = \left(\hat{\mathbf{x}}_{k-1}, \delta_{1k} \mathbf{H}^H \mathbf{y}, \delta_{2k} \mathbf{H}^H \mathbf{H} \hat{\mathbf{x}}_{k-1} \right)$$

$$\hat{\mathbf{x}}_k = g(\mathbf{d}_k)$$

$$= \rho_{L_g, k} \left(\left| \mathbf{W}_{L_g, k}^g \left(\rho_{L_g-1, k} \left(\dots \left(\rho_{1, k} \left(\left| \mathbf{W}_{1, k}^g \mathbf{d}_k^T + \mathbf{b}_{1, k}^g \right|_{bnorm} \right) \right) \dots \right) + \mathbf{b}_{L_g, k}^g \right|_{bnorm} \right),$$

where L_g , \mathbf{W}_i^g , and \mathbf{b}_i^g , have the same definitions as described for the encoder's block, only that these apply for the decoder. The decoder's input features vector, \mathbf{d}_k , was initialized by randomizing a prediction $\hat{\mathbf{x}}_0$. Initialization by zeros resulted in performance degradation.

D. Training of the CAE Network

We train a single CAE model for all tested SNR values. We use the AdamW optimizer [43] that runs back-propagation to optimize the model during training. This optimizer is designed to improve gradients when L_2 regularization is used. Our loss function is set to solve the constrained optimization problem by handling three objectives: accurate signal reconstruction (minimal BER), minimal PAPR, and acceptable ACPR.

We solve this constrained optimization problem by recasting it as an unconstrained problem by constructing the Lagrangian function and augmenting the objective function with a quadratic

penalty term [44]. The augmented Lagrangian (AL) combines the Lagrangian formulation with a weighted quadratic penalty function. The general AL for an inequality-constrained problem can be described by

$$\mathcal{F}_{\rho^k}(\mathbf{x}, \lambda^k) = f(\mathbf{x}) + \lambda_1^k c_1(\mathbf{x}) + \frac{1}{2} \rho_1^k \|c_1(\mathbf{x})\|_2^2 + \frac{1}{2\rho_2^k} \left\{ \left[\max\{0, \lambda_2^k + \rho_2^k c_2(\mathbf{x})\} \right]^2 - (\lambda_2^k)^2 \right\}, \quad (16)$$

where f denotes the objective function, $\rho^k \triangleq (\rho_1^k, \rho_2^k)$ are positive penalty parameters, $\lambda^k \triangleq (\lambda_1^k, \lambda_2^k)$ are the Lagrangian multipliers, the c_1 -involved expressions handle the equality constraint, and c_2 is for the inequality constraint. Equation (16) considers the elimination of a slack variable $s \geq 0$ that was introduced in the representation of the inequality constraint to transform it into a relaxed equality constraint. As suggested in [45], the minimizer $s = \max\{0, c_2(x) - \lambda_2 \frac{1}{\rho_2}\}$ was used. k is the iteration number for updating the Lagrangian multipliers and penalty term, according to the following rule derived by the dual ascent method [44],

$$x^{k+1} := \arg \min_x \mathcal{F}_{\rho^k}(\mathbf{x}, \lambda^k) \quad (17)$$

$$\lambda_1^{k+1} := \lambda_1^k + \rho_1^k c_1(\mathbf{x}^{k+1}) \quad (18)$$

$$\lambda_2^{k+1} := \max\{0, \lambda_2^k + \rho_2^k c_2(\mathbf{x}^{k+1})\}. \quad (19)$$

We saw better convergence and more stable results for different BO values by adding the quadratic penalty function and adaptively updating the multipliers instead of keeping them constant. Since adaptive penalty parameter update was not beneficial for the examined cases, it was added as a fixed hyperparameter.

Following the above-described general inequality constraint optimization problem, the formulation of our loss function based on the appropriate objective and constraints, represented by

four loss components \mathcal{L}_1 , \mathcal{L}_{2a} , \mathcal{L}_{2b} , and \mathcal{L}_3 , is

$$\begin{aligned} \mathcal{L}(\mathbf{x}, \hat{\mathbf{x}}, \lambda_{2a}^k, \lambda_{2b}^k, \lambda_3^k) &= \mathcal{L}_1(\mathbf{x}, \hat{\mathbf{x}}) + \lambda_{2a}^k \mathcal{L}_{2a}(\mathbf{x}) + \frac{\rho_{2a}}{2} \|\mathcal{L}_{2a}(\mathbf{x})\|_2^2 \\ &+ \lambda_{2b}^k \mathcal{L}_{2b}(\mathbf{x}) + \frac{\rho_{2b}}{2} \|\mathcal{L}_{2b}(\mathbf{x})\|_2^2 + \frac{1}{2\rho_3} \left\{ [\max\{0, \lambda_3^k + \rho_3 \mathcal{L}_3(\mathbf{x})\}]^2 - (\lambda_3^k)^2 \right\}, \end{aligned} \quad (20)$$

where λ_{2a} , λ_{2b} , λ_3 , ρ_{2a} , ρ_{2b} , and ρ_3 are the appropriate Lagrange multipliers and penalty parameters, accordingly. These are considered hyper-parameters, which balance the contribution of each loss component to the joint loss function. We start with a moderate value of λ_{2a} , λ_{2b} and λ_3 and then iterate for a better value according to the resulting PAPR loss of each iteration and some predetermined PAPR threshold value. Better performance was observed for relatively small λ_{2b} values, with very low ρ_{2b} , meaning that λ_{2b} was kept almost constant during training.

The loss function we use for optimizing the signal reconstruction and detection is the sum of negative log loss function of the predicted output probability of the real and imaginary parts of each symbol, with L_2 regularization to reduce over-fitting. Denoting by x the input sample (which is also the output target), \hat{x} as the estimated signal, Θ as the model's weights, and λ_1 as a hyperparameter for tuning the L_2 regularization, the loss function for each OFDM MIMO sample is given by,

$$\begin{aligned} \mathcal{L}_1(\mathbf{x}, \hat{\mathbf{x}}) &= - \left[\sum_{j=1}^{N_t} \sum_{s=1}^{N_{sc}} \sum_{q=1}^{N_c} 1 \left\{ Re\{x^j\} = l_q \right\} \log P_\theta \left(Re\{\hat{x}^j\} = l_q \right) \right. \\ &\quad \left. + \sum_{j=1}^{N_t} \sum_{s=1}^{N_{sc}} \sum_{q=1}^{N_c} 1 \left\{ Im\{x^j\} = l_q \right\} \log P_\theta \left(Im\{\hat{x}^j\} = l_q \right) \right] + \lambda_1 \|\Theta\|_2^2, \end{aligned} \quad (21)$$

where $N_c = \sqrt{|\mathcal{M}|}$ denotes the number of the real value possibilities, l_q , of each of the real and imaginary parts of the transmitted modulated symbol.

The PAPR minimization part is handled with two loss components, where one, \mathcal{L}_{2a} , is calculated according to the BPF input, x_n^E , and the other one, \mathcal{L}_{2b} , according to the BPF output,

x_n^F (cf. Fig. 3a). These are our equality constraints, defined by

$$\mathcal{L}_{2a}(x) = \text{PAPR}\{x_n^E\}, \quad (22)$$

$$\mathcal{L}_{2b}(x) = \text{PAPR}\{x_n^F\}. \quad (23)$$

Other than the role of PAPR minimization handled by either of the components, $\mathcal{L}_{2a}(x)$, significantly improved the BER result together with the ACPR, while $\mathcal{L}_{2b}(x)$, enabled us to control and obtain better spectral performance, meaning lower ACPR with lower output back-off (OBO) values. The ACPR loss component is given by

$$\mathcal{L}_3(x) = \text{ACPR}\{x_n^P\} - \text{ACPR}_{\text{req}}, \quad (24)$$

where x_n^P is the PA's output, and ACPR_{req} is the required ACPR value, which is usually dictated by a standard. ACPR_{req} was set according to the 5G standard requirements for high spectral purity: $\text{ACPR}_{\text{req}} \leq -45\text{dB}$ [6]; thus, $\mathcal{L}_3(x)$ defines our inequality constraint.

We have applied a gradual loss learning technique. In the first stage, the loss function consisted only of \mathcal{L}_1 and optimized only the reconstruction loss. Then, after a predetermined number of epochs, the loss function defined in (20) was used to reduce the PAPR and improve the spectral behavior. The gradual loss learning enables better control and stability in tuning the different criteria' trade-offs.

IV. RESULTS AND INSIGHTS

A. Data Generation and Experimental Setup

To train and test the proposed data-driven model, the MATLAB[®] 5G Toolbox[™] [46] was used. This toolbox provides 5G radio-standard-compliant functions to generate accurate data for MIMO-OFDM transmission, according to specified constellation sizes and examined MIMO setups. MIMO-OFDM transmissions over fading channels were simulated, where TDL-D type channels - a 13 delay tap channel with a 30ns delay spread, as described in the 3gpp specification document [6], were used for our implemented algorithm.

We consider a MIMO-OFDM system with $K = 72$ subcarriers over 14 OFDM symbols per frame. 4375 batches of 32 MIMO samples each were used for a single training set, where the input and output of the CAE sample shape is $[2/4 - \text{antennas}, (72 - \text{subcarriers}) \times (2 - \text{complex - parts}) \times (4 - \text{oversampling})]$. An oversampling factor $L = 4$, and smoothness factor $p = 2$ were considered. We trained three identical CAE models on the following setups:

- 1) QPSK modulation scheme with a 2×2 MIMO setting, with 3GPP multipath channel.
- 2) 16-QAM modulation scheme with a 4×4 MIMO setting, with 3GPP multipath channel.
- 3) 16-QAM modulation scheme with a 4×4 MIMO setting, with AWGN channel.

To provide an unbiased performance evaluation of the final training model, the training and test data sets were generated independently, i.e. OFDM symbols, channel realization, and noise were randomized independently. In the following, we give numerical performance results of our multi-objective CAE model compared to a classical CF algorithm with a clipping ratio of 4.08 dB, and to SLM with $U = 64$ phase sequences, with MLE added for MIMO detection. The inference part was performed on 7000 MIMO samples for each SNR point.

B. Training Setup

As a part of the experimental analysis, we performed an extensive exploration of different model structures and hyper-parameters, including the number of layers, kernel sizes, number of convolutional layer channels, regularization, dropout, number of decoder iterations, batch-normalization, learning rate, AL parameters, trained SNR value, and epoch number. We found that the best performance versus complexity on both examined MIMO setups was achieved for the same model structure, only with different training data sets. As the constellation, the number of subcarriers per OFDM symbols, and the number of antennas are higher, the training is longer, and it is harder to achieve the desired results. The proposed CAE structure for the above 4×4 MIMO system is described in Table I, where $\lambda_{2a}^{(0)}$, $\lambda_{2b}^{(0)}$, and $\lambda_3^{(0)}$ are the values of the first iteration when the AL epochs start, and 'Grad start' indicates the number of initial epochs where only the reconstruction loss is counted, optimizing the unconstrained problem. 'LR' indicates the learning

TABLE I: CAE Proposed Structure

Parameter	Transmitter				Receiver			
	Value	Kernel	Ch-in	Ch-out	Value	Kernel	Ch-in	Ch-out
Input size	4×720	-	-	-	12×144	-	-	-
Conv (SELU)	-	1×3	1	21	-	3×3	1	15
Conv (SELU)	-	1×3	21	15	-	3×3	15	21
Conv (SELU)	-	1×3	15	21	-	-	-	-
FC (Linear) output size	4×720	-	-	-	12×144	-	-	-
Decoder iterations	-	-	-	-	10	-	-	-

Conv padding	LR	Epochs num	Grad start	SNR train	$\lambda_{2a}^{(0)}, \lambda_{2b}^{(0)}, \lambda_3^{(0)}$	$\rho_{2a}, \rho_{2b}, \rho_3$
2	0.001	140	45	40 dB	0.015, 0.001, 0.005	0.0015, 0.00001, 0.001

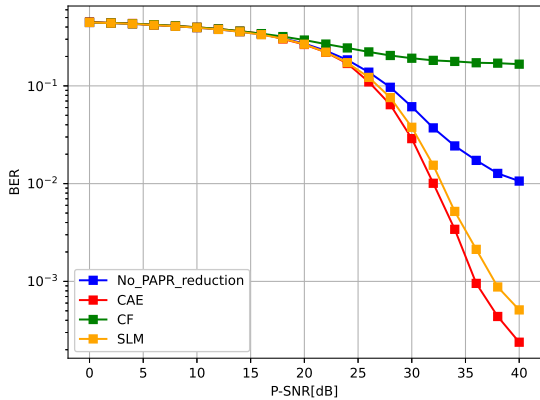
rate. Training on any of the data sets with the same best SNR value used for noise generation, 'SNR train', showed the top overall inference performance for any tested SNRs. Adding dropout had no benefit in all examined setups.

C. BER Analysis

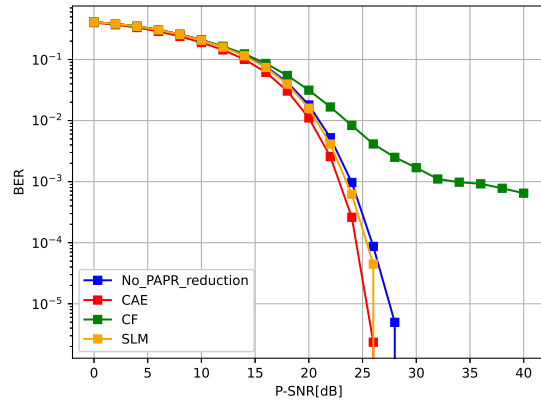
The calculation of BER versus Peak Signal to Noise Ratio (P_SNR) is used here as a key parameter to measure the reconstruction and detection of the transmitted signal. Considering a normalized channel, i.e. $\mathbb{E} \|\mathbf{H}\|^2 = 1$, the P_SNR is defined as the ratio between the MIMO system maximal emitted energy, P_T , and the noise power, σ_w^2 , such that

$$\text{P_SNR} = \frac{P_T}{\sigma_w^2}. \quad (25)$$

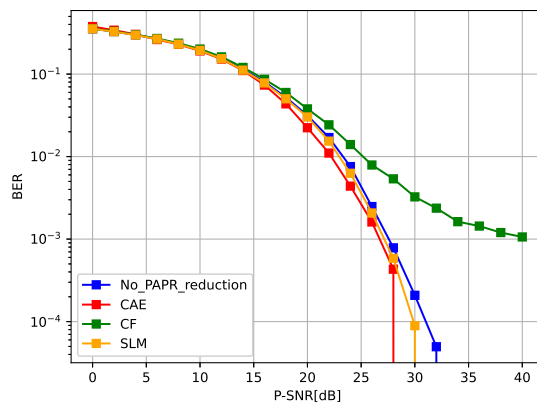
As shown in Fig. 4, the CAE has competitive BER vs. P_SNR performance compared to the other standard examined methods in most of the P_SNR range, where a visible gain is achieved at the higher part. As the NN does not assume any specific physical model, it has better robustness to distortions. That is, the MIMO-OFDM signal reconstruction and detection of HPA-distorted data as a part of the multi-objective optimization proposed by our end-to-end DL scheme has the benefit over the common algorithms.



(a) 16-QAM, 4x4 MIMO with 3GPP multipath channel



(b) 16-QAM, 4x4 MIMO with AWGN channel

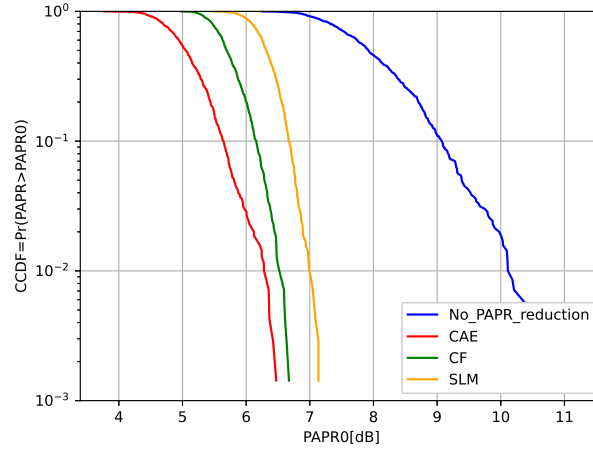
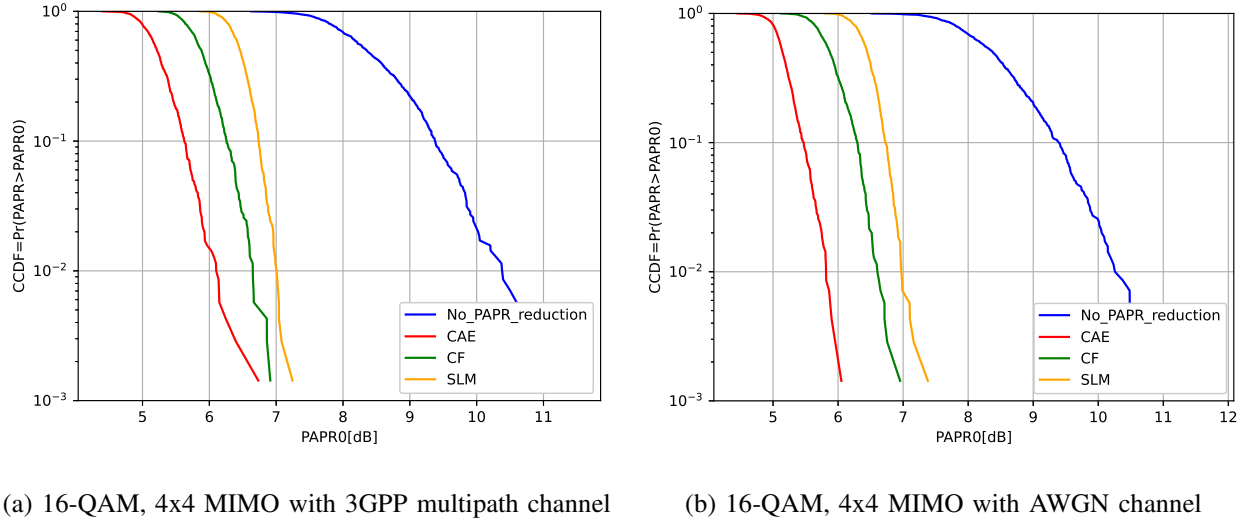


(c) 4-QAM, 2x2 MIMO with 3GPP multipath channel

Fig. 4: BER vs. P_SNR of the considered methods and setups.

D. CCDF for PAPR Comparison

To demonstrate the PAPR performance of different methods, complementary cumulative distribution function (CCDF) curves are presented in Fig. 5. The CCDF of the PAPR denotes the probability that the PAPR exceeds a certain threshold, i.e. $\mathbb{P}(\text{PAPR}_{\text{MIMO-OFDM}} > \text{PAPR}_0)$. The PAPR is calculated according to the BPF output, x_n^F . As can be observed in Fig. 5, the proposed CAE achieves the better performance of PAPR reduction compared to the CF and SLM methods. However, still the BER and spectral behavior are more important for performance evaluation.



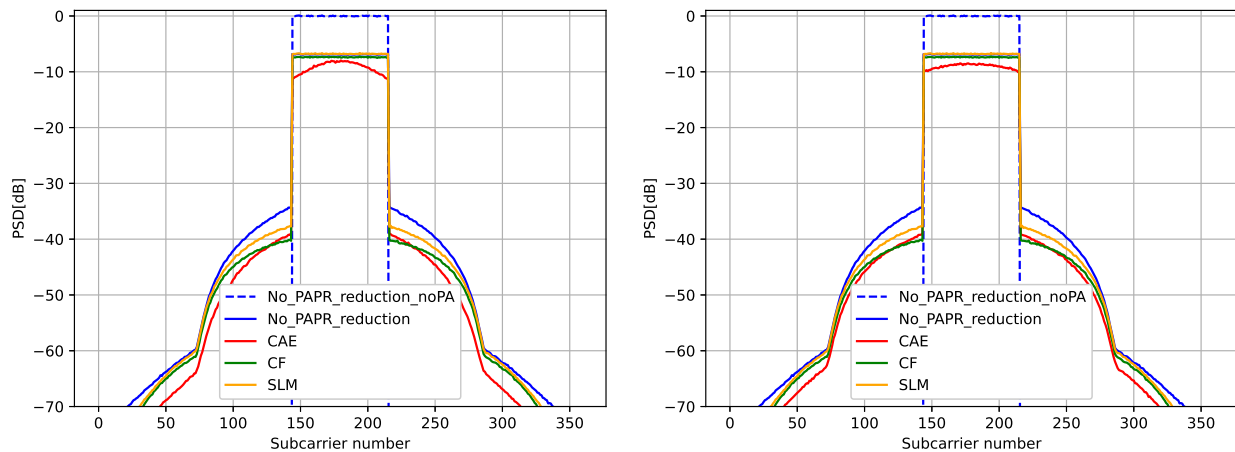
(c) 4-QAM, 2x2 MIMO with 3GPP multipath channel

Fig. 5: CCDF of PAPR of the considered methods.

E. Spectrum Analysis

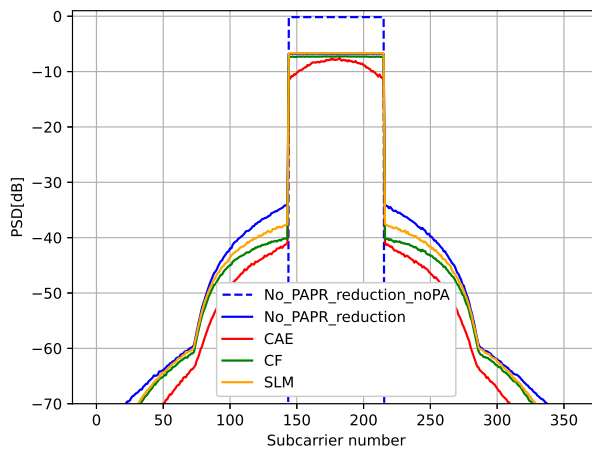
Figure 6 compare the spectral performance in terms of the PSD of the transmitted signals for all examined methods. The dashed rectangle shows perfect spectral behavior for a linear HPA with no non-linear components.

The proposed CAE decreases the out-of-band distortions at the expense of lower transmitted power efficiency. Observing the spectral behavior as a part of the experimental analysis showed us that there is a trade-off between increasing the IBO and increasing the Lagrange multiplier associated with the PAPR loss component, λ_{2b} . As shown in Fig. 7, while increasing the IBO mostly shifts the CAE curve downwards, increasing λ_{2b} causes the curve to bend more.



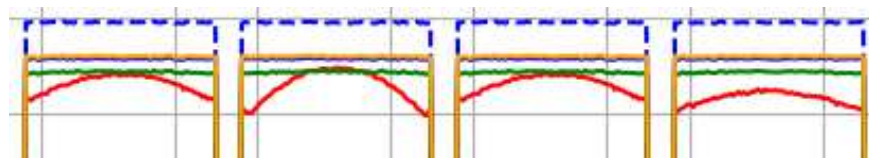
(a) 16-QAM, 4x4 MIMO with 3GPP multipath channel

(b) 16-QAM, 4x4 MIMO with AWGN channel



(c) 4-QAM, 2x2 MIMO with 3GPP multipath channel

Fig. 6: PSD for the considered methods.

(a) moderate λ_{2b} (b) high λ_{2b}

(c) moderate IBO

(d) high IBO

Fig. 7: Spectral mask behavior trade-off between IBO and λ_{2b} .

The transmitter's OBO, which evaluates the power efficiency of the system, is defined as the ratio between the maximal radiated power that is the maximal power transmitted by all the HPAs in the network, P_T , and the mean transmitted power at the HPAs' input, i.e.

$$\text{OBO} = \frac{P_T}{\sum_{m=1}^{N_t} \mathbb{E}(|x_{n,m}^B|^2)}. \quad (26)$$

TABLE II: ACPR and OBO

Parameter	4QAM 2X2 MIMO					16QAM 4X4 MIMO				
	CAE	FC-AE	CF	SLM	No-reduction	CAE	FC-AE	CF	SLM	No-reduction
ACPR[dB]	-39.87	-37.26	-39.08	-37.73	-34.99	-37.88	-36.53	-39.004	-37.67	-35.01
OBO[dB]	5.92	6.62	6.74	6.78	6.86	6.09	6.77	6.74	6.78	6.84

The maximum radiated power is defined to be $P_T = 1$. P_T is divided equally between the HPAs. In other words, the maximal transmitted power of each HPA is P_T/N_t . As we defined all HPAs to have the same characteristics, the saturation level of each HPA is $A_0 = \sqrt{P_T/N_T}$. Table II compares the ACPR and the OBO of the proposed CAE to the other methods. As shown, the ACPR of the CAE is comparable with the considered methods.

In Fig. 8 we further compare the OBO performance for different ACPR values. It can be seen that the CAE system requires lower OBOs, which is better overall power efficiency, while maintaining better BER compared to the other methods.

F. Autoencoder - FC vs. CNN

We investigated various NN types for the AE, in particular, FC and CNN. Figure 9a compares the BER performance of two AE architectures: the proposed CAE, which contains convolutional layers, and a fully connected autoencoder (FC-AE), which contains only FC layers. It can be observed that the CAE network has better BER performance compared to the FC-AE. As shown in Table II, the ACPR of the CAE is better than that of the FC-AE. Moreover, the CAE has lower complexity and thus faster training. The three convolutional layers have a total of 1953 parameters, while for three FC layers of sizes 3500, 2500, and 3500, as were used for the FC-AE

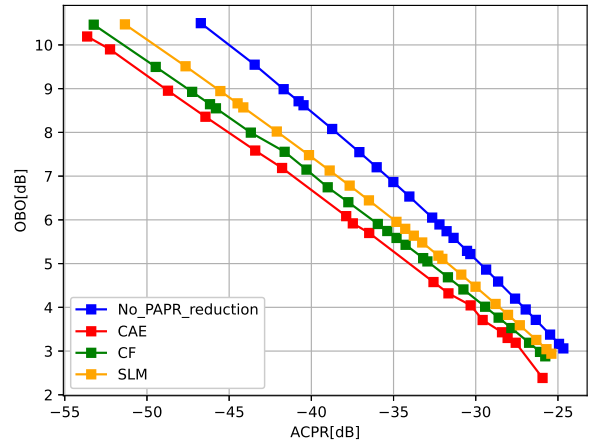


Fig. 8: OBO vs. ACPR for the considered methods for 16-QAM with 4x4 MIMO setup and 3GPP multipath channel.

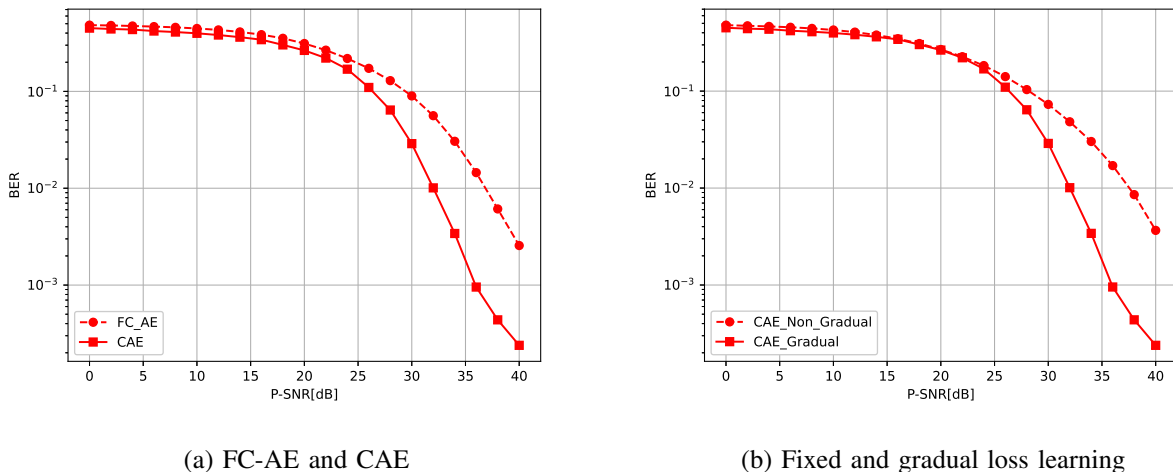


Fig. 9: BER vs. P_SNR learning approaches comparison of 16-QAM, 4x4 MIMO with 3GPP multipath channel.

in Fig. 9a and Table II, the number of parameters is around 10^7 .

G. Fixed vs. Gradual Loss Learning

To show the benefits of using a gradual loss learning procedure, Fig. 9b compares its BER performance to that of a fixed-loss training procedure, where the loss function's weights are fixed for the entire training. It can be observed that the gradual loss learning procedure significantly improves the BER. In addition, improving the BER while keeping the PAPR and spectral performance at the desired levels is easier to control when applying the gradual loss learning method than manipulating loss function weights in fixed-loss training. Also, spectral performance and PAPR reduction were harder to control and provide similar performance.

V. CONCLUSIONS AND FUTURE WORK

In this study, we have presented a CAE model for PAPR reduction and waveform design in a MIMO-OFDM communication system. We have applied a gradual loss learning method to optimize the performance in terms of three objectives: low BER, low PAPR, and adherence to ACPR spectral requirements, on top of the AL multipliers optimization technique. The presented CAE structure trainable parts included a neural PAPR reduction block, followed by a BPF filter to optimize the spectral behavior at the transmitter, and a neural iterative MIMO detection block at

the receiver, both were simultaneously optimized as a part of the end-to-end network design. The proposed CAE was shown to outperform the CF and the SLM algorithms at the examined cases. Future work can extend the MIMO scenario to higher modulation schemes and larger MIMO setups, aiming to achieve a functional utility for future wireless communication networks.

REFERENCES

- [1] T. Jiang and G. Zhu, "Complement block coding for reduction in peak-to-average power ratio of ofdm signals," *IEEE Communications Magazine*, vol. 43, no. 9, p. S17–S22, 2005.
- [2] M. Z. Chowdhury, M. Shahjalal, S. Ahmed, and Y. M. Jang, "6g wireless communication systems: Applications, requirements, technologies, challenges, and research directions," *IEEE Open Journal of the Communications Society*, vol. 1, pp. 957–975, 2020.
- [3] A. Bo, Y. Zhi-Xing, P. C.-Y. Z. Tao-Tao, and G. Jian-Hua, "Effects of papr reduction on hpa predistortion," *IEEE Transactions on Consumer Electronics*, vol. 51, no. 4, pp. 1143–1147, 2005.
- [4] C.-X. Wang, M. D. Renzo, S. Stanczak, S. Wang, and E. G. Larsson, "Artificial intelligence enabled wireless networking for 5g and beyond: Recent advances and future challenges," *IEEE Wireless Communications*, vol. 27, no. 1, pp. 16–23, 2020.
- [5] Y. S. Cho, J. Kim, W. Y. Yang, and C. G. Kang, *MIMO-OFDM wireless communications with MATLAB*. John Wiley & Sons, 2010.
- [6] 3GPP, "3rd generation partnership project (3gpp). study on channel model for frequencies from 0.5 to 100 ghz," 3rd Generation Partnership Project (3GPP), Technical Specification (TS). [Online]. Available: https://www.3gpp.org/ftp/Specs/archive/38_series/38.901
- [7] B. Hassibi and H. Vikalo, "On sphere decoding algorithm 1: expected complexity," *IEEE Transaction on Signal Processing*, vol. 53, no. 8, pp. 2806–2818, 2005.
- [8] P. W. Wolniansky, G. J. Foschini, G. D. Golden, and R. A. Valenzuela, "V-blast: An architecture for realizing very high data rates over the rich-scattering wireless channel," in *1998 URSI international symposium on signals, systems, and electronics. Conference proceedings (Cat. No. 98EX167)*. IEEE, 1998, pp. 295–300.
- [9] B. Steingrimsson, Z.-Q. Luo, and K. M. Wong, "Soft quasi-maximum-likelihood detection for multiple-antenna wireless channels," *IEEE Transactions on Signal Processing*, vol. 51, no. 11, pp. 2710–2719, 2003.
- [10] N. Samuel, T. Diskin, and A. Wiesel, "Learning to detect," *IEEE Transactions on Signal Processing*, vol. 67, no. 10, pp. 2554–2564, 2019.
- [11] O. Sholev, H. H. Permuter, E. Ben-Dror, and W. Liang, "Neural network MIMO detection for coded wireless communication with impairments," in *2020 IEEE Wireless Communications and Networking Conference (WCNC)*, 2020, pp. 1–8.
- [12] M. Mohammadkarimi, M. Mehrabi, M. Ardakani, and Y. Jing, "Deep learning-based sphere decoding," *IEEE Transactions on Wireless Communications*, vol. 18, no. 9, pp. 4368–4378, 2019.

- [13] K. Pratik, B. D. Rao, and M. Welling, "Re-mimo: Recurrent and permutation equivariant neural mimo detection," *IEEE Transactions on Signal Processing*, vol. 69, pp. 459–473, 2020.
- [14] T. J. O'Shea, T. Erpek, and T. C. Clancy, "Deep learning based mimo communications," *arXiv preprint arXiv:1707.07980*, 2017.
- [15] J. Song, C. Häger, J. Schröder, T. J. O'Shea, E. Agrell, and H. Wymeersch, "Benchmarking and interpreting end-to-end learning of mimo and multi-user communication," *IEEE Transactions on Wireless Communications*, 2022.
- [16] T. O'shea and J. Hoydis, "An introduction to deep learning for the physical layer," *IEEE Transactions on Cognitive Communications and Networking*, vol. 3, no. 4, pp. 563–575, 2017.
- [17] M. A. Albreem, M. Juntti, and S. Shahabuddin, "Massive mimo detection techniques: A survey," *IEEE Communications Surveys & Tutorials*, vol. 21, no. 4, pp. 3109–3132, 2019.
- [18] I. Gutman, I. Iofedov, and D. Wulich, "Iterative decoding of iterative clipped and filtered OFDM signal," *IEEE Transactions on Communications*, vol. 61, no. 10, pp. 4284–4293, 2013.
- [19] A. P. More and S. B. Somani, "The reduction of PAPR in OFDM systems using clipping and SLM method," in *2013 International Conference on Information Communication and Embedded Systems (ICICES)*, 2013, pp. 593–597.
- [20] Di-xiao Wu, "Selected mapping and partial transmit sequence schemes to reduce PAPR in OFDM systems," in *2011 International Conference on Image Analysis and Signal Processing*, 2011, pp. 1–5.
- [21] T. Jiang and Y. Wu, "An overview: Peak-to-average power ratio reduction techniques for OFDM signals," *IEEE Transactions on Broadcasting*, vol. 54, no. 2, pp. 257–268, 2008.
- [22] A. Mobasher and A. K. Khandani, "Integer-based constellation-shaping method for PAPR reduction in OFDM systems," *IEEE Transactions on Communications*, vol. 54, no. 1, pp. 119–127, 2006.
- [23] Z. Q. Taha and X. Liu, "An adaptive coding technique for PAPR reduction," in *IEEE GLOBECOM 2007 - IEEE Global Telecommunications Conference*, 2007, pp. 376–380.
- [24] Y. Lee, Y. You, W. Jeon, J. Paik, and H. Song, "Peak-to-average power ratio in mimo-ofdm systems using selective mapping," *IEEE Communications Letters*, vol. 7, no. 12, pp. 575–577, 2003.
- [25] A. Namitha and S. Sameer, "A bandwidth efficient selective mapping technique for the papr reduction in spatial multiplexing mimo-ofdm wireless communication system," *Physical Communication*, vol. 25, pp. 128–138, 2017.
- [26] A. Zappone, M. Di Renzo, and M. Debbah, "Wireless networks design in the era of deep learning: Model-based, AI-based, or both?" *IEEE Transactions on Communications*, vol. 67, no. 10, pp. 7331–7376, 2019.
- [27] I. Sohn, "A low complexity PAPR reduction scheme for OFDM systems via neural networks," *IEEE Communications Letters*, vol. 18, no. 2, pp. 225–228, 2014.
- [28] I. Sohn and S. C. Kim, "Neural network based simplified clipping and filtering technique for PAPR reduction of OFDM signals," *IEEE Communications Letters*, vol. 19, no. 8, pp. 1438–1441, 2015.
- [29] M. Kim, W. Lee, and D. Cho, "A novel papr reduction scheme for OFDM system based on deep learning," *IEEE Communications Letters*, vol. 22, no. 3, pp. 510–513, 2018.

- [30] L. Shi, X. Zhang, W. Wang, Z. Wang, A. Vladimirescu, Y. Zhang, and J. Wang, "PAPR reduction based on deep autoencoder for VLC DCO-OFDM system," in *2019 IEEE International Symposium on Broadband Multimedia Systems and Broadcasting (BMSB)*, 2019, pp. 1–4.
- [31] Y. Huleihel, E. Ben-Dror, and H. H. Permuter, "Low papr waveform design for ofdm systems based on convolutional autoencoder," in *2020 IEEE International Conference on Advanced Networks and Telecommunications Systems (ANTS)*. IEEE, 2020, pp. 1–6.
- [32] F. A. Aoudia and J. Hoydis, "Waveform learning for next-generation wireless communication systems," *IEEE Transactions on Communications*, 2022.
- [33] L. Hao, D. Wang, W. Cheng, J. Li, and A. Ma, "Performance enhancement of ACO-OFDM-based VLC systems using a hybrid autoencoder scheme," *Optics Communications*, vol. 442, pp. 110–116, 2019.
- [34] A. Kalinov, R. Bychkov, A. Ivanov, A. Osinsky, and D. Yarotsky, "Machine learning-assisted papr reduction in massive mimo," *IEEE Wireless Communications Letters*, vol. 10, no. 3, pp. 537–541, 2020.
- [35] A. Ivanov and D. Lakontsev, "Selective tone reservation for papr reduction in wireless communication systems," in *2017 IEEE International Workshop on Signal Processing Systems (SiPS)*. IEEE, 2017, pp. 1–6.
- [36] A. Ivanov, A. Volokhatyi, D. Lakontsev, and D. Yarotsky, "Unused beam reservation for papr reduction in massive mimo system," in *2018 IEEE 87th Vehicular Technology Conference (VTC Spring)*. IEEE, 2018, pp. 1–5.
- [37] P. Kenington, "Methods linearize RF transmitters and power amps," *Microwaves & RF*, vol. 37, no. 13, pp. 102–116, 1998.
- [38] S. Santurkar, D. Tsipras, A. Ilyas, and A. Madry, "How does batch normalization help optimization?" in *Advances in Neural Information Processing Systems*, 2018, pp. 2483–2493.
- [39] K. He, X. Zhang, S. Ren, and J. Sun, "Deep residual learning for image recognition," in *Proceedings of the IEEE conference on computer vision and pattern recognition*, 2016, pp. 770–778.
- [40] G. Klambauer, T. Unterthiner, A. Mayr, and S. Hochreiter, "Self-normalizing neural networks," in *Advances in neural information processing systems*, 2017, pp. 971–980.
- [41] H. E. Rowe, "Memoryless nonlinearities with gaussian inputs: Elementary results," *The BELL system technical Journal*, vol. 61, no. 7, pp. 1519–1525, 1982.
- [42] G. L. Stuber, J. R. Barry, S. W. McLaughlin, Y. Li, M. A. Ingram, and T. G. Pratt, "Broadband mimo-ofdm wireless communications," *Proceedings of the IEEE*, vol. 92, no. 2, pp. 271–294, 2004.
- [43] I. Loshchilov and F. Hutter, "Decoupled weight decay regularization," *arXiv preprint arXiv:1711.05101*, 2017.
- [44] S. Boyd, N. Parikh, E. Chu, B. Peleato, and J. Eckstein, "Distributed optimization and statistical learning via the alternating direction method of multipliers," *Foundations and Trends® in Machine learning*, vol. 3, no. 1, pp. 1–122, 2011.
- [45] D. G. Luenberger and Y. Yinyu, *Linear and nonlinear programming*. Springer, 1984, vol. 2.
- [46] "Matlab 5g toolbox," 2020, the MathWorks, Natick, MA, USA. [Online]. Available: <https://www.mathworks.com/products/5g.html>